materials

MDPI

Article

High Responsivity MgZnO Ultraviolet Thin-Film Phototransistor Developed Using Radio Frequency Sputtering

Jyun-Yi Li, Sheng-Po Chang *, Ming-Hung Hsu and Shoou-Jinn Chang

Department of Electrical Engineering and Advanced Optoelectronic Technology Center, Institute of Microelectronics, National Cheng Kung University, Tainan 701, Taiwan; z823040@gmail.com (J.-Y.L.); hsuminghung0121@gmail.com (M.-H.H.); changsj@mail.ncku.edu.tw (S.-J.C.)

* Correspondence: changsp@mail.ncku.edu.tw; Tel.: +886-6-2757575 (ext. 62391)

Academic Editor: Pedro Barquinha

Received: 27 September 2016; Accepted: 24 January 2017; Published: 4 February 2017

Abstract: We investigated the electrical and optoelectronic properties of a magnesium zinc oxide thin-film phototransistor. We fabricate an ultraviolet phototransistor by using a wide-bandgap MgZnO thin film as the active layer material of the thin film transistor (TFT). The fabricated device demonstrated a threshold voltage of 3.1 V, on–off current ratio of 10^5, subthreshold swing of 0.8 V/decade, and mobility of 5 $cm^2/V{\cdot}s$ in a dark environment. As a UV photodetector, the responsivity of the device was 3.12 A/W, and the rejection ratio was 6.55×10^5 at a gate bias of -5 V under 290 nm illumination.

Keywords: magnesium zinc oxide; ultraviolet; thin-film transistor; phototransistor

1. Introduction

In recent years, ultraviolet photodetectors have attracted much attention for their potential in medical, commercial, and military applications [1–5]. The thin-film transistor (TFT) has been intensively researched for its application to switching devices in large-area display panels (active matrix liquid crystal displays (AMLCDs) and organic light-emitting diodes). A number of different materials are utilized for TFT fabrication. Many groups have used ZnO-based semiconductors as the TFT channel layer, owing to their high field mobility, low temperature processing, and nontoxicity. Oxide TFTs with photosensitive metal oxide semiconductor materials are promising candidates that can act as photodetectors. Bae et al. reported the fabrication of a ZnO-based phototransistor [6]. Zan et al. reported on an amorphous IGZO (a-IGZO) visible-light photodetector with a polymeric light absorption layer [7]. Chiu et al. reported the fabrication of deep-UV-sensitive a-IGZO TFTs with a Ta_2O_5 gate dielectric [8]. However, the electrical properties and material characteristics of the TFT's active layer strongly influence the device's transfer characteristics. TFTs with a ZnO active layer exhibit n-type conductivity owing to the oxygen vacancies and zinc interstitials. Thus, defect density control is the key to the performance of ZnO-based TFTs [9–12]. Magnesium zinc oxide is emerging as a TFT active layer candidate because its large bandgap can decrease donor-like defects [13,14]. In addition, the strong bonding energy between magnesium and oxide reduces oxygen vacancies, which makes Mg a good candidate for doping into ZnO for the TFT active layer. In several studies, TFTs with MgZnO have been fabricated with various processing methods, such as radio frequency-sputtering with a 5% Mg target [15], e-beam evaporation with 1% Mg content [16], and atomic layer deposition with 10% Mg content [17]. Because of its wide direct bandgap, the MgZnO material system is an excellent choice for optoelectronic devices in the UV portion of the spectrum. MgZnO also possesses unique figures of merit such as intrinsic visible blindness and radiation hardness that are crucial for practical

optoelectronic devices. Hullavarad et al. reported that the UV/visible rejection ratio—defined as the ratio of the photoresponse at 310–800 nm—is 10^4 for $Mg_{0.15}Zn_{0.85}O$ on Al_2O_3 and 10^3 on quartz substrates. In addition, solar or visible–blind $Mg_xZn_{1-x}O$ photodetectors have been fabricated on sapphire, glass, and silicon substrates [18]. Photodetectors fabricated on $Mg_{0.68}Zn_{0.32}O/SrTiO_3/Si$ have demonstrated the peak photoresponse at 225 nm and a UV/visible rejection ratio that is only one order of magnitude [19]. Prototype $Mg_xZn_{1-x}O$ UV photodetectors with different Mg contents have been fabricated with high photoresponsivities and sharp cutoffs at ~375, ~350, ~315, and ~300 nm for x values of 0, 0.10, 0.26, and 0.34, respectively [20]. Magnesium doping suppresses the subthreshold current. Furthermore, the magnesium atom also exists at interstitials in the crystal and forms impurity scattering centers, which leads to poor TFT mobility and a large threshold voltage. Nonetheless, there have been few studies related to MgZnO TFTs, let alone their fabrication via radio frequency-sputtering.

In this work, we investigated the properties of MgZnO TFTs that are fabricated by radio frequency-sputtering with different oxygen flow ratios, and then generalized the optimized conditions. We extended the application of the TFTs to a phototransistor to combine the photoelectrical properties of MgZnO and the transistor to increase the responsivity. Under the optimal parameters, the MgZnO TFT can operate normally, and the device has high mobility, a fast on–off transition, and high responsivity under deep UV illumination.

2. Materials and Methods

First, to fabricate MgZnO TFTs, 2 cm × 2 cm glass substrates were cleaned with acetone, isopropyl alcohol, and deionized (DI) water. Figure 1 shows the cross-section of the MgZnO TFT. The aluminum bottom gate was thermally deposited on a quartz substrate (Sunmei Glass Company, Taiwan, China). Next, a 200 nm thick SiO_2 layer—which acted as a dielectric—was deposited by using the plasma-enhanced chemical vapor deposition (PECVD) process (PD-220NA, SAMCO, Kyoto, Japan). The 10-nm-thick MgZnO channel was fabricated from a MgZnO (MgO = 10 wt%, ZnO = 90 wt%) target (GfE Gesellschaft für Elektrometallurgie mbH: GfE, Nürnberg, Germany). During channel layer sputtering, the chamber pressure was kept at 10 mTorr, the sputtering power was fixed at 100 W, and the substrates were rotated at a speed of 20 rpm. The oxygen flow ratio was varied from 0% to 21% in increments of 7% (i.e., 0%, 7%, 14%, and 21%). After the channel layer deposition, the samples were placed in a furnace for annealing for 30 min at 300 °C. This was done to incorporate the magnesium atoms into the crystal lattice. The source and drain electrodes were deposited on the MgZnO active layer by thermal evaporation. The width/length (W/L) of the active layer was fixed at 1000 μm/100 μm. The current-voltage (I–V) characteristics of the fabricated TFTs were measured in the dark at room temperature and atmospheric pressure with a B1500 semiconductor parameter analyzer (Agilent Technologies, Santa Clara, CA, USA). The parameters of the TFTs were calculated by using Equation (1).

The mobility of our TFTs was determined in the saturation region. In the saturation region, the drain current can be represented by

$$I_D = \frac{W}{2L} C\mu (V_G - V_t)^2, \quad (1)$$

where C is the capacitance of the dielectric layer (~16.8 nF·cm^{-2}); W is the channel width; L is the channel length; V_t and V_G are the threshold voltage and gate voltage respectively; and μ is the field-effect mobility. We used the gate width-length (W/L) ratio of 10. The subthreshold swing (*S.S.*) is defined as

$$S.S. = \frac{\partial V_G}{\partial \log I_D}, \quad (2)$$

where V_G and I_D are the gate voltage and drain current respectively. The small value of *S.S.* was attributed to both the high gate capacitance density and high interface charge density. The photoresponsivity of the fabricated device was measured with a 250 W Xe lamp dispersed

by a monochromator as the light source. The monochromatic light, which was calibrated with a UV-enhanced Si diode and optical power meter, was modulated by a mechanical chopper and then collimated on the front side of the fabricated device with an optical fiber. The illumination area was 0.1 mm^2.

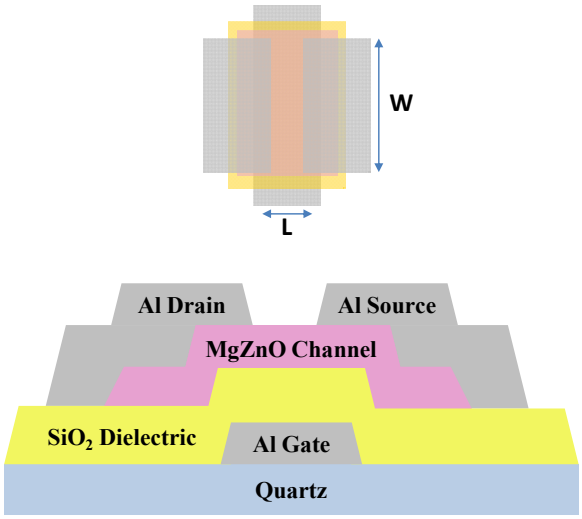

Figure 1. Top view and cross-section of the MgZnO thin-film transistor (TFT). W, channel width; L, channel length.

3. Results and Discussion

As for the film optical properties, the transmittance and optical bandgap determined by the absorption coefficient were considered. Figure 2 shows the transmittance spectra of the MgZnO thin film with various oxygen flow ratios. The transmittance in the visible region could clearly be more than 80%. The absorption edge of the MgZnO thin film was from 329 nm to 334 nm. The inset depicts the relationship between absorption coefficient and photon energy. The energy bandgap of MgZnO was found to be around 3.43 eV, regardless of the oxygen flow ratio.

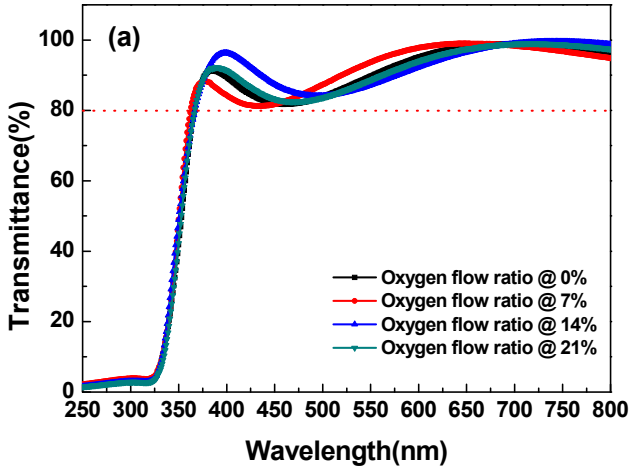

Figure 2. *Cont.*

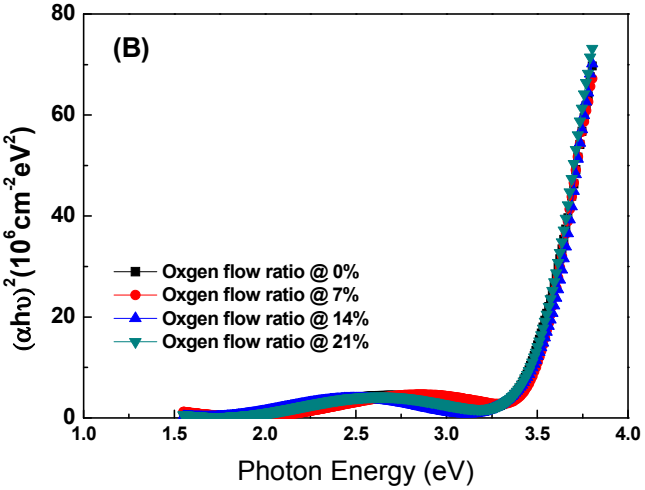

Figure 2. (**A**) Transmittances of the MgZnO thin film with a variable oxygen flow ratio of 0%–21%, (**B**) Absorption coefficient versus the photon energy for MgZnO thin film with a variable oxygen flow ratio of 0%–21%.

The variation in the oxygen ratio hardly affected the absorption edge. When oxygen gas was not introduced during sputtering, more defects developed in the MgZnO thin film. Accordingly, changes in the sputtering oxygen flow ratio were considered to determine the compensation level of the oxygen vacancies.

Figure 3 shows the transfer characteristics of the TFTs with various oxygen flow ratios, and Table 1 lists the parameters. Table 1 indicates that samples with an oxygen flow ratio of 14% exhibit the best characteristics. The MgZnO TFT with a 0% oxygen flow ratio had more defects compared with the other samples, leading to poor electrical properties. When the oxygen flow ratio increased, the properties were gradually improved. The oxygen flow ratio of 14% reduced the oxygen vacancies in the crystal properly however, the oxygen flow ratio of 21% caused the formation of acceptor-like defects owing to the excessive oxygen. This conclusion can also be obtained from the difference in *S.S.* for various oxygen flow ratios. When the flow ratio was 14%, the TFT had the lowest *S.S.* and a relatively small total trap density. At an ideal oxygen flow ratio, the on–off ratio could be up to five orders of magnitude.

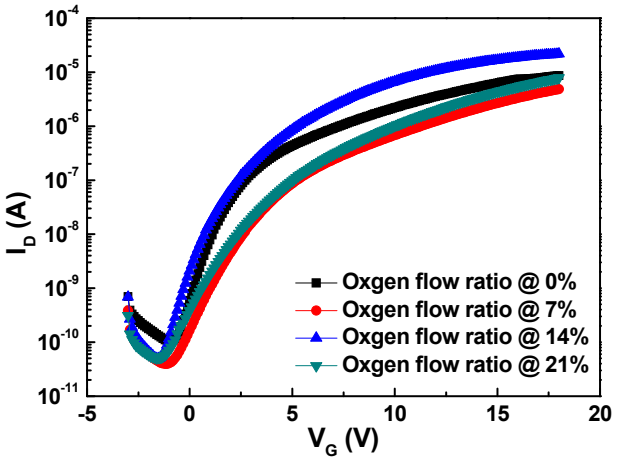

Figure 3. Transfer characteristics of the MgZnO TFT.

Table 1. Transfer characteristics of the MgZnO TFT with various oxygen ratios.

Oxygen Ratio	V_t (V)	μ_{eff} (cm^2/Vs)	On–Off Current Ratio	*S.S.*	N_t
0%	3.6 ± 0.072	2.42 ± 0.048	$8.4 \times 10^4 \pm 1680$	0.89 ± 0.018	1.6×10^{12}
7%	6.6 ± 0.132	2.17 ± 0.043	$1.2 \times 10^5 \pm 2400$	1.65 ± 0.033	2.9×10^{12}
14%	3.1 ± 0.062	5.65 ± 0.113	$4.4 \times 10^5 \pm 8800$	0.80 ± 0.016	1.4×10^{12}
21%	6.2 ± 0.124	3.25 ± 0.065	$1.5 \times 10^5 \pm 3300$	1.36 ± 0.027	2.4×10^{12}

V_t, threshold voltage; μ_{eff}, field-effect mobility; *S.S.*, subthreshold swing; N_t, trapping density.

Figure 4 shows the XPS spectra of O 1s for films grown at different oxygen flow ratios from 7% to 21%. The peak at the lower binding energy of ~530 eV (O_I) was attributed to O^{2-} ions present in a stoichiometric wurtzite MgZnO structure. The peak at the higher binding energy of ~532 eV (O_{II}) was is attributed to oxygen deficiencies in MgZnO [21]. This result shows that, as the flow ratio increased from 7% to 14% the oxygen in the films tended to compensate for the vacancies in the crystal lattice. This can be confirmed by the spectrum curve area decreasing from 75.3% to 65.3%. However, as the sputtering oxygen flow ratio was increased to 21%, the oxygen composition in the film became defective, which contributed to undesirable oxygen interstitials. The spectrum area at the higher binding energy increased from 65.3% to 81.3%, which is related to the difference in the *S.S.* of various oxygen flow ratios. When the flow ratio was 14%, the TFT had the lowest *S.S.* and a relatively low total trap density.

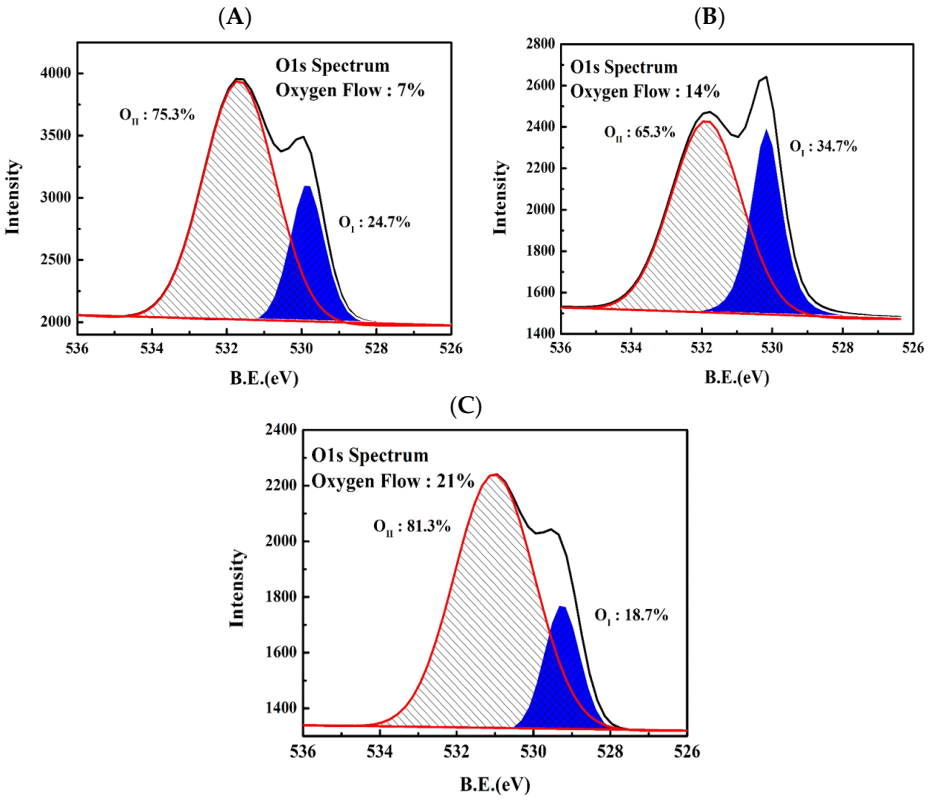

Figure 4. X-ray photoelectron spectroscopy (XPS) O 1s spectrum of a MgZnO thin film sputtered with oxygen flow ratios of (**A**) 7%; (**B**) 14%; and (**C**) 21%.

Oxide TFTs with photosensitive metal oxide semiconductor materials can be used as phototransistors, which are key components in optoelectronic circuits. Hence, we exposed the MgZnO TFTs to light to analyze the photo characteristics. Figure 5 shows the transfer characteristics for the

oxygen flow ratio of 14% for an MgZnO TFT in the dark and under illumination from 450 nm to 250 nm when plotted as a function of V_G from −10 V to 25 V, with drain voltage (V_D) fixed at 12 V. Under illumination, the threshold voltage had a significant negative shift, and the drain current increased owing to the photo-generation from excessive holes and free electrons. Therefore, I_d of the MgZnO TFT illuminated with UV light (whose photon energy is greater than the bandgap of the semiconducting material) has two components: (i) the current flowing between the source/drain electrodes (I_{ds}) because of the applied bias voltage, and (ii) the photoconductive component (I_{ph}):

$$I_d = I_{ds} + I_{ph}. \tag{3}$$

I_{ph} is given by the relation

$$I_{ph} = \frac{q(\mu_n)\eta F_{ph}\tau_p W V_{DS}}{L}, \tag{4}$$

where μ_n is electron mobility, η is the quantum efficiency, F_{ph} is the photon flux, τ_p is the carrier lifetime, q is the electronic charge, W and L are the width and length of the device, respectively, and V_{DS} is the voltage applied between the source and drain electrodes [22]. Thus, for a given photon flux F_{ph}, the photoconductive component will be large if V_{DS} is large. Hence, with the corresponding threshold voltage shift, the transistor is easier to turn on. The drain current was enhanced in the wavelength range between 300 and 350 nm, which corresponds to the optical characteristics of MgZnO.

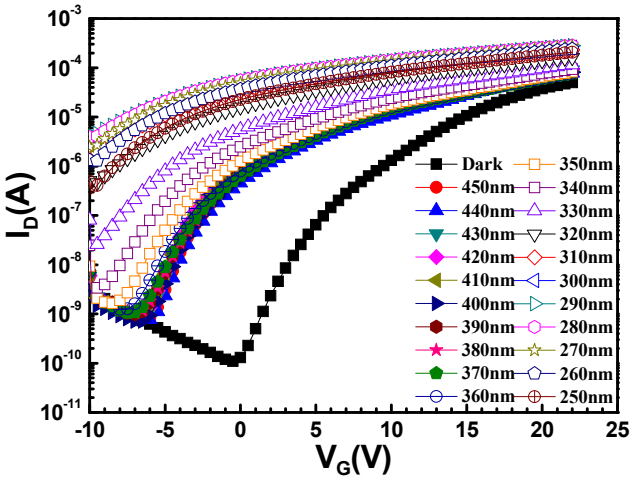

Figure 5. I_D–V_G output characteristics of an MgZnO thin-film phototransistor under illumination.

Figure 6 shows the spectral response of the fabricated MgZnO device. Here, we define the UV-to-visible rejection ratio as the responsivity measured at 290 nm divided by the responsivity measured at 450 nm:

$$Rejection\ Ratio\ (R.R.) = \frac{Responsivity\ (290\ \text{nm})}{Responsivity\ (450\ \text{nm})} \tag{5}$$

UV-to-visible rejection ratio of a photodetector measures the ability of a device to detect UV light signals compared to visible light signals. The value of UV-to-visible rejection ratio is the responsivity of a certain wavelength of UV light region divided by the responsivity of a certain wavelength of visible light region. If the rejection ratio is high, it implies that the device is more sensitive to UV light. We pursue the goal of accomplishing a photodetector with high UV-to-visible rejection ratio. With an incident light wavelength of 290 nm and an applied gate bias of −5 V, the measured responsivity of the device was 3.12 A/W, and the UV-to-visible rejection ratio was 6.55×10^5. Such result again indicates that the fabricated TFT was very UV-sensitive and can be used as a solar-blind phototransistor.

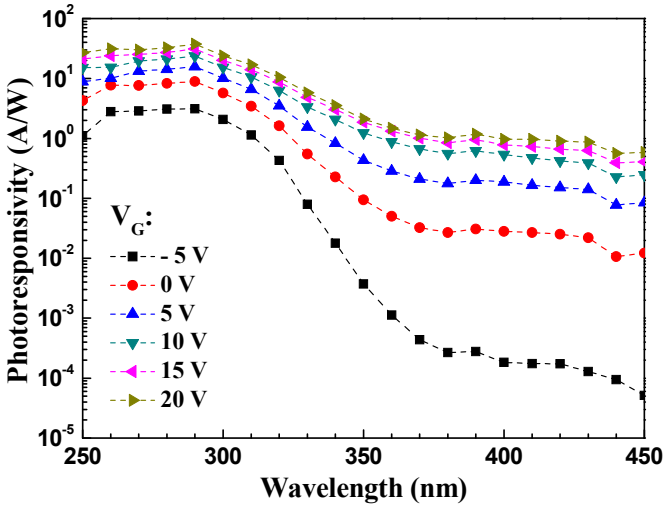

Figure 6. Photoresponsivity spectra of the MgZnO thin-film phototransistor with a bias of −5 V to 20 V under different light illumination.

4. Conclusions

The best characteristics of the MgZnO TFT with a SiO_2 dielectric were obtained with a sputtering oxygen flow rate controlled at 14% in order to compensate for the oxygen vacancies. Under this condition, the transistor exhibited an on–off ratio of five orders of magnitude, and a mobility of ~5 cm^2/Vs was achieved. Our results broaden the applicability of MgZnO TFTs to photodetectors. When a negative gate bias was applied, the optimized MgZnO phototransistor exhibited fine photo properties. The responsivity of the device was 3.12 A/W, and the rejection ratio was 6.55 × 10^5 at a gate bias of −5 V under 290 nm illuminations. The results indicate that the fabricated device is suitable for solar-blind photodetectors.

Acknowledgments: This work was supported by the Ministry of Science and Technology under contract number MOST 103-2221-E-006-098 and MOST 105-2221-E-006-118. This work was also supported in part by the Center for Frontier Materials and Micro/Nano Science and Technology, National Cheng Kung University, Taiwan, and by the Advanced Optoelectronic Technology Center, National Cheng Kung University, for projects from the Ministry of Education.

Author Contributions: Jyun-Yi Li, Sheng-Po Chang conceived and designed the experiments; Jyun-Yi Li, Sheng-Po Chang, Ming-Hung Hsu, Shoou-Jinn Chang performed the experiments; Jyun-Yi Li, Sheng-Po Chang, Ming-Hung Hsu, Shoou-Jinn Chang analyzed the data; Jyun-Yi Li, Sheng-Po Chang, Ming-Hung Hsu, Shoou-Jinn Chang wrote the paper.

Conflicts of Interest: The authors declare no conflict of interest.

References

1. Chai, G.; Lupan, O.; Chow, L.; Heinrich, H. Crossed zinc oxide nanorods for ultraviolet radiation detection. *Sensor. Actuat. A Phys.* **2009**, *150*, 184–187. [CrossRef]
2. Osinsky, A.; Gangopadhyay, S.; Gaska, R.; Williams, B.; Khan, M.A.; Kuksenkov, D.; Temkin, H. Low noise p-π-n GaN ultraviolet photodetectors. *Appl. Phys. Lett.* **1997**, *71*, 2334–2336. [CrossRef]
3. Smith, C.A.; Lee, H.W.H.; Leppert, V.J.; Risbud, S.H. Ultraviolet-blue emission and electron-hole states in ZnSe quantum dots. *Appl. Phys. Lett.* **1999**, *75*, 1688–1690. [CrossRef]
4. He, J.H.; Lin, Y.H.; McConney, M.E.; Tsukruk, V.V.; Wang, Z.L.; Bao, G. Enhancing UV photoconductivity of ZnO nanobelt by polyacrylonitrile functionalization. *J. Appl. Phys.* **2007**, *102*, 084303. [CrossRef]
5. Gimenez, A.J.; Yáñez-Limón, J.M.; Seminario, J.M. ZnO–cellulose composite for UV sensing. *IEEE Sens. J.* **2013**, *13*, 1301–1306. [CrossRef]
6. Bae, H.S.; Yoon, M.H.; Kim, J.H.; Im, S. Photodetecting properties of ZnO-based thin-film transistors. *Appl. Phys. Lett.* **2003**, *83*, 5313–5315. [CrossRef]

7. Zan, H.W.; Chen, W.T.; Hsueh, H.W.; Kao, S.C.; Ku, M.C.; Tsai, C.C.; Meng, H.F. Amorphous indium-gallium-zinc-oxide visible-light phototransistor with a polymeric light absorption layer. *Appl. Phys. Lett.* **2010**, *97*, 203506. [CrossRef]
8. Chiu, C.J.; Weng, W.Y.; Hsueh, T.J.; Chang, S.J.; Huang, G.J.; Hsueh, H.T. Ta_2O_5 Solar-Blind Photodetectors. *IEEE Sens. J.* **2011**, *11*, 2372–2373. [CrossRef]
9. Zhang, S.B.; Wei, S.H.; Zunger, A. Intrinsic n-type versus p-type doping asymmetry and the defect physics of ZnO. *Phys. Rev. B* **2001**, *63*, 075205. [CrossRef]
10. Furuta, M.; Kamada, Y.; Kimura, M.; Hiramatsu, T.; Matsuda, T.; Furuta, H.; Li, C.; Fujita, S.; Hirao, T. Analysis of Hump Characteristics in Thin-Film Transistors With ZnO Channels Deposited by Sputtering at Various Oxygen Partial Pressures. *IEEE Electron Device Lett.* **2010**, *31*, 1257–1259.
11. Kimura, M.; Nakanishi, T.; Nomura, K.; Kamiya, T.; Hosono, H. Trap densities in amorphous-$InGaZnO_4$ thin-film transistors. *Appl. Phys. Lett.* **2008**, *92*, 133512. [CrossRef]
12. Su, L.Y.; Lin, H.Y.; Wang, S.L.; Yeh, Y.H.; Cheng, C.C.; Peng, L.H.; Huang, J.J. Effects of gate-bias stress on ZnO thin-film transistors. *J. Soc. Inf. Disp.* **2010**, *18*, 802–806. [CrossRef]
13. Chin, H.A.; Cheng, I.C.; Huang, C.I.; Wu, Y.R.; Lu, W.S.; Lee, W.L.; Lin, T.S. Two dimensional electron gases in polycrystalline MgZnO/ZnO heterostructures grown by rf-sputtering process. *J. Appl. Phys.* **2010**, *108*, 054503. [CrossRef]
14. Kwon, Y.; Li, Y.; Heo, Y.W.; Jones, M.; Holloway, P.H.; Norton, D.P.; Park, Z.V.; Li, S. Enhancement-mode thin-film field-effect transistor using phosphorus-doped (Zn,Mg)O channel. *Appl. Phys. Lett.* **2004**, *84*, 2685–2687. [CrossRef]
15. Li, C.H.; Tsai, Y.S.; Chen, J.Z. Negative bias temperature instability of Rf-sputtered Mg0.05Zn0.95O thin film transistors with MgO gate dielectrics. *Semicond. Sci. Tech.* **2011**, *26*, 105007. [CrossRef]
16. Wu, H.; Liang, J.; Jin, G.; Lao, Y.; Xu, T. Transparent thin-film transistors using ZnMgO as dielectrics and channel. *IEEE Trans. Electron Devices* **2007**, *54*, 2856–2859. [CrossRef]
17. Wrench, J.S.; Brunell, I.F.; Chalker, P.R.; Jin, J.D.; Shaw, A.; Mitrovic, I.Z.; Hall, S. Compositional tuning of atomic layer deposited MgZnO for thin film transistors. *Appl. Phys. Lett.* **2014**, *105*, 202109. [CrossRef]
18. Hullavarad, S.S.; Dhar, S.; Varughese, B.; Takeuchi, I.; Venkatesan, T.; Vispute, R.D. Realization of Mg (x = 0.15) Zn (1 − x = 0.85) O-based metal-semiconductor-metal UV detector on quartz and sapphire. *J. Vac. Sci. Technol. A* **2005**, *23*, 982–985. [CrossRef]
19. Yang, W.; Vispute, R.D.; Choopun, S.; Sharma, R.P.; Venkatesan, T.; Shen, H. Ultraviolet photoconductive detector based on epitaxial Mg0.34Zn 0.66O thin films. *Appl. Phys. Lett.* **2001**, *78*, 2787–2789. [CrossRef]
20. Koike, K.; Hama, K.; Nakashima, I.; Takada, G.Y.; Ogata, K.I.; Sasa, S.; Inoue, M.; Yano, M. Molecular beam epitaxial growth of wide bandgap ZnMgO alloy films on (111)-oriented Si substrate toward UV-detector applications. *J. Cryst. Growth* **2005**, *278*, 288–292. [CrossRef]
21. Hwang, D.K.; Lee, K.; Kim, J.H.; Im, S.; Park, J.H.; Kim, E. Comparative studies on the stability of polymer versus SiO_2 gate dielectrics for pentacene thin-film transistors. *Appl. Phys. Lett.* **2006**, *89*, 093507. [CrossRef]
22. Hong, W.K.; Kim, B.J.; Kim, T.W.; Jo, G.; Song, S.; Kwon, S.S.; Yoon, A.; Stach, E.A.; Lee, T. Electrical properties of ZnO nanowire field effect transistors by surface passivation. *Colloid. Surface. A* **2008**, *313*, 378–382. [CrossRef]